Winter 12-19-2018

Modeling of Cantú Syndrome in Zebrafish

Soma Sekhara Singareddy
Washington University in St. Louis

WASHINGTON UNIVERSITY IN ST. LOUIS

School of Engineering and Applied Science

Department of Biomedical Engineering

Thesis Examination Committee:
Colin G. Nichols, Chair
Jonathan R. Silva
Nathaniel Huebsch

A Thesis on

Modeling of Cantú Syndrome in Zebrafish

by

Soma Sekhara Singareddy

A thesis presented to the School of Engineering
of Washington University in St. Louis in partial fulfillment of the
requirements for the degree of
Master of Science

December 2018

Saint Louis, Missouri

Contents

List of Figures

List of Tables

Acknowledgments

I take great pleasure in thanking Prof. Colin G. Nichols, my guide and research mentor for this project, who continues to support, motivate and kindle me with intellectual inquiry.

I express my gratefulness to Conor McClenaghan, whose phenomenal enthusiasm to practice science coupled with his benevolent personality, kept the project going forward even in dire situations.

The immediate gratitude goes to Helen Roessler, for all the efforts during our collaboration, without whom, this project wouldn't exist.

My sincere thanks go to Rob Tryon, for his valuable help, without which the project would be a clutter.

I'm hugely indebted to all the distinguished researchers within Nichols' lab for their crucial suggestions and regular feedback that proved very essential to this project.

Special thanks to Prof. Jonathan Silva and Prof. Nathaniel Huebsch for their positive criticism that helped strengthen the related research.

Soma Sekhara Singareddy

Washington University in St. Louis

December 2018

ABSTRACT OF THE THESIS

A Thesis on

Modeling of Cantú Syndrome in Zebrafish

by

Soma Sekhara Singareddy

Master of Science in Biomedical Engineering

Washington University in St. Louis, 2018

Research Advisor: Professor Colin G. Nichols

Although rare, Cantú syndrome (CS) is a debilitating syndrome without any specific therapy, caused by gain-of-function (GOF) mutations in *KCNJ8* and *ABCC9* genes that encode ATP-sensitive potassium (K_{ATP}) channels. To better understand the link between molecular dysfunction and the complex pathophysiology, animal models that can rigorously mirror human CS are essential. Using *ABCC9*-mutated zebrafish, which can provide significant advantages over mice as an appropriate vertebrate model, GOF has been demonstrated at a cellular level in the ventricular cardiomyocytes. This also marks the first-known characterization of K_{ATP} currents in teleost hearts. In addition, sulfonylurea sensitivities of the channels have been studied, along with phenotypic consequences of such treatment, exploring a potential therapeutic approach to treating CS.

Chapter 1

Introduction

Historically, animal models have been used to better understand human physiology and anatomy. Advances in the field of genetics have enabled the replication of the genetic basis of human disease in animal models to study development and progression of various gene-specific diseases affecting the humans, as well as to test new treatments [1, 11]. One such understudied disease is 'Cantú Syndrome'.

1.1 Cantú Syndrome

Hypertrichotic osteochondrodysplasia, commonly known as Cantú syndrome (CS), named after the Mexican physician José Maria "Chema" Cantú, who first delineated the disease [2], is a rare genetic disorder characterized by excessive hair growth (hypertrichosis), distinctive facial appearance (large head, broad nasal bridge, epicanthal folds and a wide mouth), enlarged heart (cardiomegaly), patent ductus arteriosus (PDA), pericardial effusion, pulmonary hypertension, skeletal abnormalities (thickening of calvaria, broad ribs, scoliosis and flaring of the metaphyses), vascular dilation and tortuosity [2, 3] (Figure 1.1).

Despite its complex pathophysiology, the molecular basis of CS has been recognized in the last 5 years as the results of gain-of-function (GOF) mutations in just two genes, either ABCC9 or KCNJ8, which encode the SUR2 sulfonylurea receptor and pore-forming Kir6.1 subunit, respectively, of ATP-sensitive potassium (K_{ATP}) channels [4-9]. That mutations in either subunit of the channel lead to the same disease is suggestive that the disorder arises from increased K_{ATP} channel activity, as opposed to any non-electrophysiological function of either subunit. Recent studies using mice models have demonstrated GOF *in vivo* and provide encouraging results that help us to better understand the connection between molecular dysfunction and the complex pathophysiology of CS [10].

Distinctive Facial Appearance

Hypertrichosis

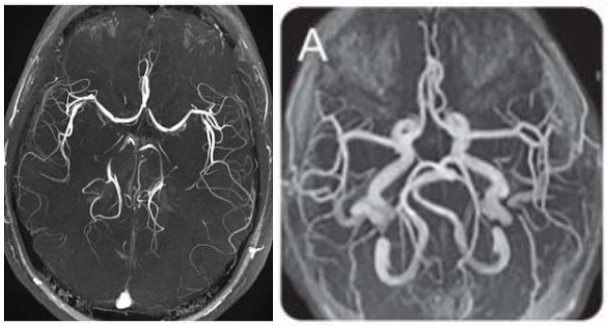

Range of Diverse CV Phenotypes
(Tortuous and dilated vasculature in the circle of Willis of a CS patient (right), contrasted with normal (left))

PDA, Pericardial Effusion, Pulmonary Hypertension

Figure 1.1 Pathophysiology of Cantú Syndrome

1.2 K_{ATP} Channels

ATP-sensitive potassium (K_{ATP}) channels are hetero-octameric potassium-selective ion channels composed of 4 pore-forming inwardly rectifying Kir6.x subunits (Kir6.1 or Kir6.2 encoded by *KCNJ8* and *KCNJ11*, respectively) and 4 regulatory sulfonylurea receptor SURx subunits (subfamily C: SUR1, SUR2 encoded by *ABCC8* and *ABCC9*), whose molecular heterogeneity is further increased by variable splicing of SUR2 into two distinct isoforms: SUR2A and SUR2B [12-18]. *KCNJ8* and *ABCC9* are an adjacent gene-pair on chromosome 12p12.1, with *KCNJ11* and *ABCC8* paralogous on 11p15.1 Regulated by intracellular nucleotides and membrane phospholipids, K_{ATP} channels serve as electrical transducers of the metabolic state of the cell by coupling cellular metabolism to the membrane potential [19]. By binding to the Kir6.x subunit, ATP decreases the channel's open probability, whereas magnesium-nucleotide complexes (MgADP and MgATP) bind to the nucleotide-binding domains (NBDs) of the SURx subunits and increase the channel open probability [20, 21] (Figure 1.2).

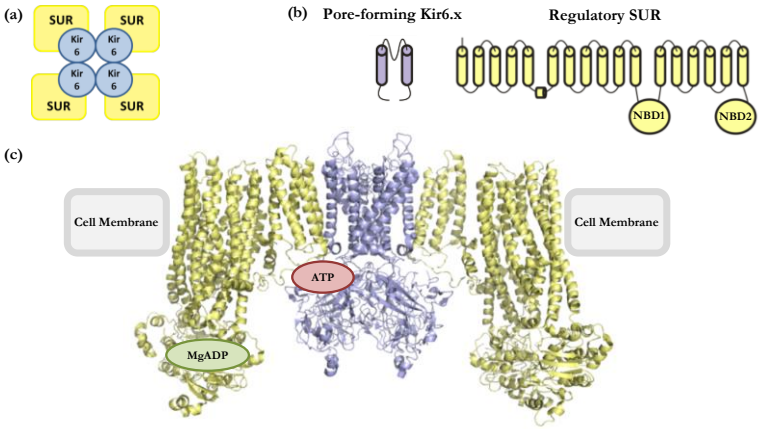

Figure 1.2 K_{ATP} Channel Structure

(a) Hetero-octameric protein complex of the K_{ATP} channel, showing Kir6 tetramer surrounded by 4 SUR subunits (b) Schematic representation of Kir6.x and SUR protein topologies, indicating the two nucleotide binding domains (NBD1 and NBD2) of SUR (c) Structural model of the complex, showing the ATP and MgATP binding sites

K_{ATP} channels are widely expressed throughout the body, primarily in the plasma membranes and through their transduction of cellular metabolic states, serve a diverse range of key functions such as ischemic pre-conditioning in the cardiomyocytes, protection against fiber damage in skeletal muscle, vasomotor control in vascular smooth muscle (VSM), regulation of insulin secretion in pancreatic β cells and determination of nerve-fiber excitability in central nervous system [22-28]. K_{ATP} channels in different tissues exhibit distinct nucleotide sensitivities as a result of distinct compositions. In pancreas and neurons, Kir6.2 is coupled with SUR1, Kir6.2 is coupled with SUR2A in the striated muscles and Kir6.1 is coupled with SUR2B in VSM [29-33] (Figure 1.3). CS mutations have been reported thus far in SUR2 and Kir6.1 domains, making it predominantly a cardiovascular disease.

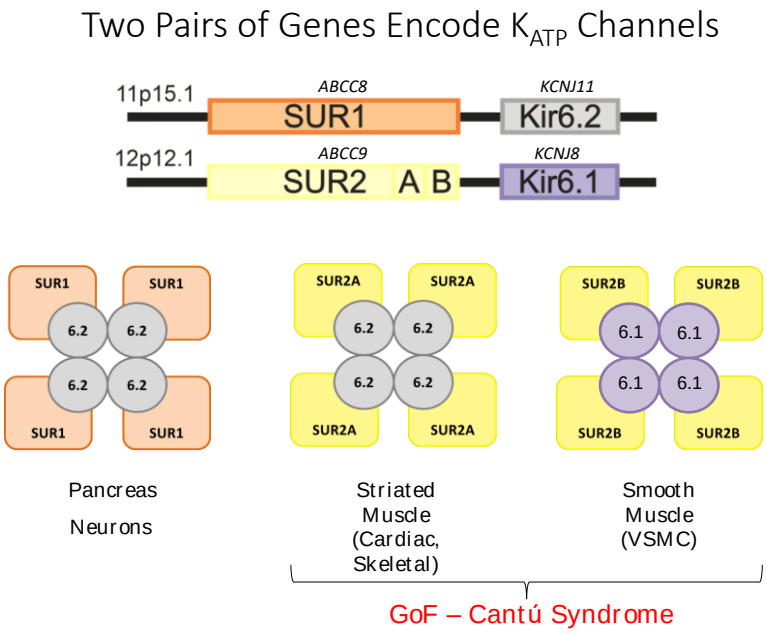

Figure 1.3 K_{ATP} Channel Composition

1.3 Zebrafish

Zebrafish (ZF; *Danio rerio*) are small freshwater teleost fish which have been used as a model organism since the 1960s. The complete genome sequence of ZF, published in 2013, has propelled its use as a leading animal model for various physiological studies, including heart research [34, 35]. ZF offer many advantages as a cardiovascular model (Figure 1.4), including:

- **Highly conserved amenable genome**
    - About 70% of protein-coding human genes and 84% of genes associated with human diseases have orthologs in zebrafish genome [34]. ZF are genetically amenable to various genetic engineering techniques and as a result of the whole genome duplication that occurred early in the teleost lineage, over 3100 human genes have at least two orthologues in ZF genome [37].
- **Rapid development and fecundity**
    - ZF achieve sexual maturity within 2 to 3 months and have a large clutch size (100 to 1000 embryos per mature female). They breed readily, every 10 days making them amenable to high-throughput drug screening. They grow as much in a day as a human embryo does in a month and possess a fully developed heart at 96 hours post fertilization [35].
- **Nearly transparent larvae that survive without circulation**
    - The transparency of ZF larvae facilitates the evaluation of phenotypes and genetic reporters *in vivo*, using light microscopy (Figure 1.4). Their larvae can function without circulation for 4–5 days at the embryonic stage, obtaining oxygen through diffusion. This makes them perfectly suitable for modelling cardiac malformations that would be fatal in other mammals [35].
- **Electrophysiological similarity to human cardiomyocytes**
    - The ZF ventricular action potential (AP) is similar to that of human cardiac AP and unlike the mouse AP, exhibits a rapid depolarization upstroke followed by a long plateau phase, resulting in a QT interval similar to that of human electrocardiogram (ECG) (Figure 1.4) [36, 37].
- **Remarkable regenerative capacity**
    - While the mammalian heart is particularly resistant to regeneration after injury, ZF heart can fully regenerate without scar formation (Figure 1.4) [38, 39]. This makes ZF a salient cardiovascular model to investigate mechanisms that stimulate the cardiac regeneration.

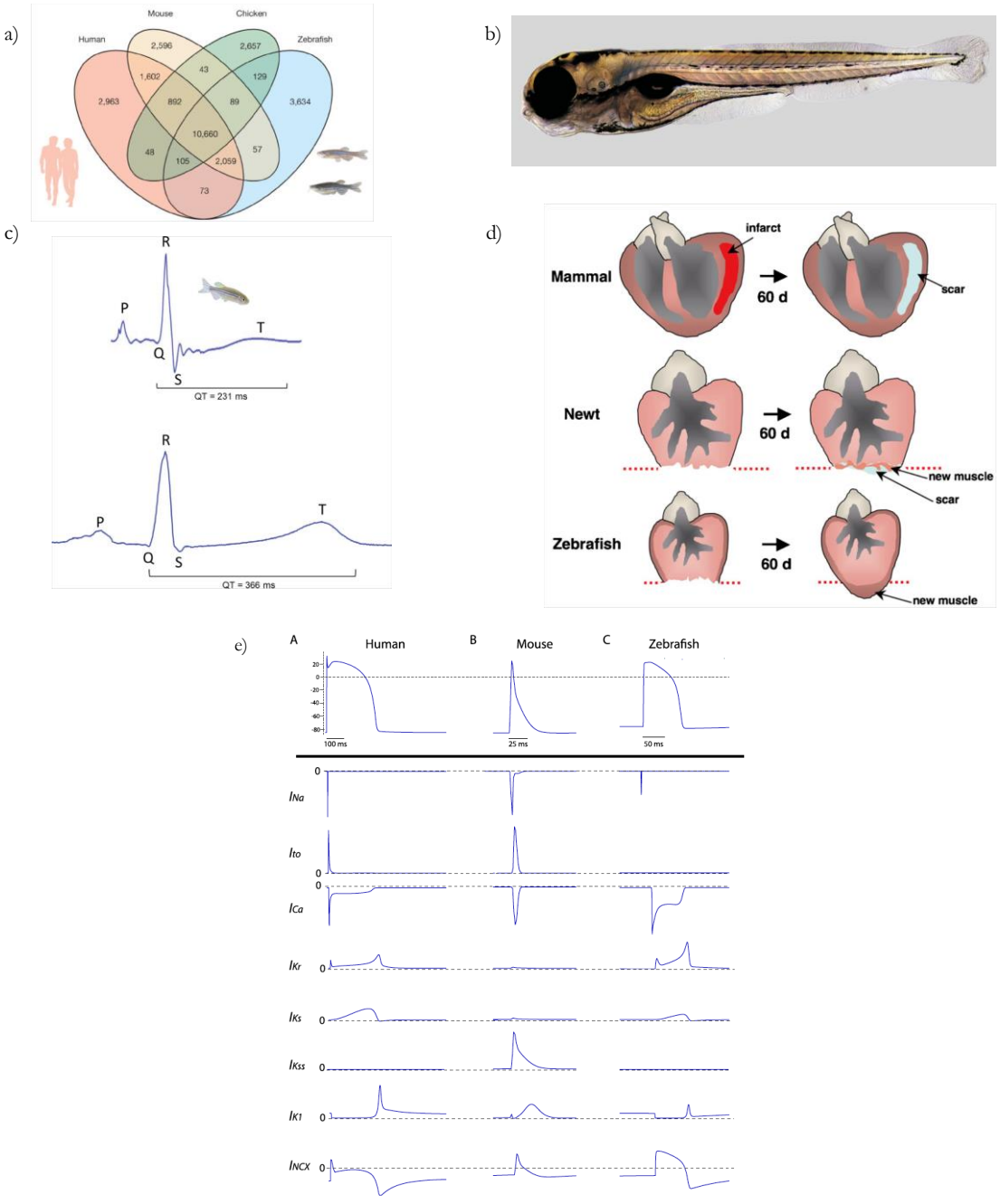

Figure 1.4 Zebrafish as a Cardiovascular Model

(a) Orthologue genes shared between ZF, human, mouse and chicken genome [34] (b) ZF larvae are nearly transparent, facilitating phenotypic evaluation using light microscopy (c) Comparison of zebrafish and human ECGs [37] (d) Typical injury models of mammalian, newt & ZF hearts [39] (e) Representative shapes of the major ion currents responsible for human, mice and zebrafish cardiac APs [36]

Chapter 2

Materials and Methods

Most ZF models developed thus far have been generated as transgenic over-expressers, which do not replicate the genetic basis of diseases caused by alleles carrying single nucleotide changes, as in CS. Using an effective approach that combined CRISPR/Cas9 with a short template oligonucleotide, Helen Roessler, in the group of Gijs van Haaften, at the University Medical Center (UMC) Utrecht, generated ZF knock-in (KI) lines carrying gain-of-function (GOF) missense mutations in SUR2-encoding ABCC9 gene and developed a ZF model for CS (Figure 2.1) [40]. Two of these lines, containing patient-specific point mutations at human orthologue locations C1043Y and G989E were used for the current study.

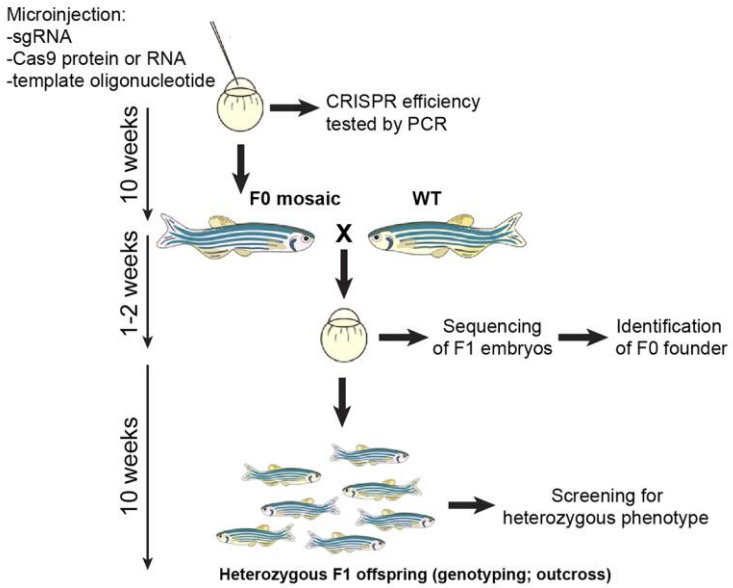

Figure 2.1 Generation of Patient-Specific KI Lines in ZF
Stepwise procedure followed to establish the knock-in lines of zebrafish [40]

2.1 Isolation of Zebrafish Ventricular Myocytes

Previous studies that implicate a physiological significance of K_{ATP} channels in ZF, were mostly performed either phenotypically or indirectly using transfected cells [41-43]. Direct analysis of ZF K_{ATP} expression and functional characterization has been performed so far only in β-cells [44]. Caveats associated with extrapolation and interpretation of such results arise from the whole genome duplication that occurred early in the teleost lineage, which suggest that molecular entities and regulatory pathways behind the functions are not always same in ZF and humans. This is evident from the recent analysis of ZF Kir2 channel composition which demonstrated striking differences between molecular basis of cardiac ionic currents (I_{K1}) in ZF and human hearts [45]. This was the rationale to determine the ZF K_{ATP} channel composition, expression and validate GOF in the developed ZF CS model at a cellular and molecular level, before any further physiological studies.

As a first step towards such validation, it was appropriate to begin with the isolation of ventricular cardiomyocytes from ZF in order to obtain recordings of channel activity in the native tissue. With only a handful of reports describing cardiomyocyte isolation from fish [46-48], this turned out to be a much more formidable task than initially expected. None of the reported protocols seemed to yield cells viable for physiological measurements. However, drawing parallels from the existing lab protocols to isolate mice and fish cardiomyocytes, I was able to develop a simple, yet effective protocol to isolate ventricular cardiomyocytes from ZF.

The protocol can be divided into 3 basic steps – Isolation, Digestion and Wash.

Isolation (Figure 2.2 [48]):

1. The fish were euthanized using cold-shock (8°C water immersion, for approximately 10 s).
2. The fish were then transferred onto a wet operation sponge (a piece of foam with incision large enough to place the fish) and placed under a dissecting microscope (Figure 2.2 a).
3. Using forceps (Dumont FST no. 5), an opening of 4 mm was carefully made in the ventral muscle longitudinally (Figure 2.2 b).

4. The heart was quickly excised and placed in heparin buffer (Table 2.1) in a 55-mm Petri dish (Figure 2.2 c).
5. Non-ventricle tissues (outflow tract, atrium, pericardium) were removed and the ventricles were gently torn open to wash out the blood (Figure 2.2 d, e).
6. The torn ventricles were then quickly transferred to 750 µl of perfusion buffer (Table 2.1) in a 1.5 ml Eppendorf tube (Figure 2.2 f).
7. A total of 3 medium-sized fish hearts were necessary for optimal cell density. The above steps were repeated for the remaining two fish and the ventricles were pooled into the same tube.
8. For best results, the isolation time for each fish heart did not exceed 90 seconds.

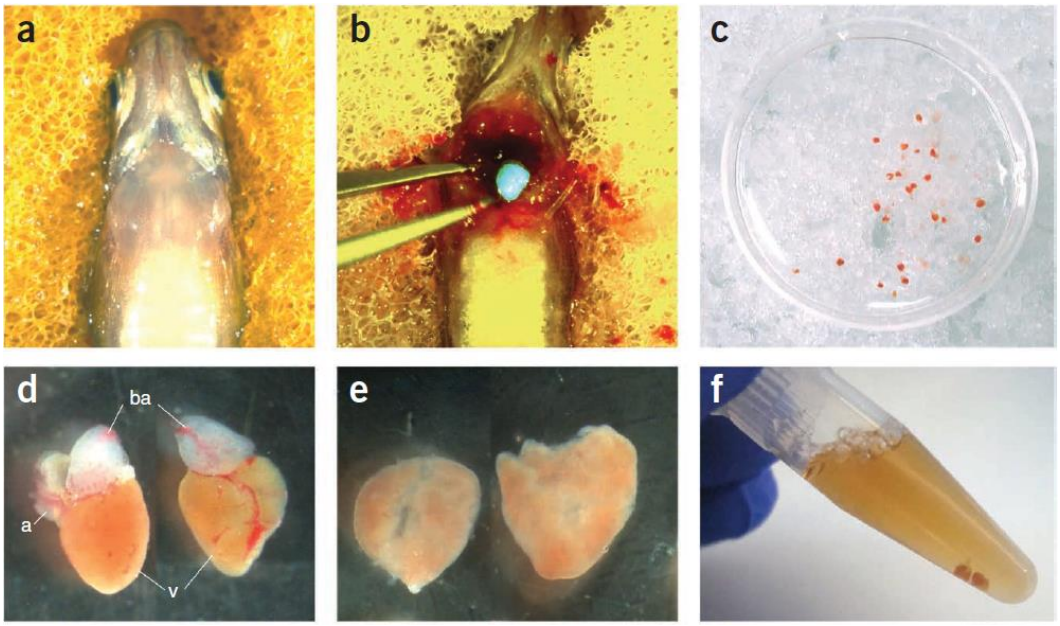

Figure 2.2 Isolation of ZF Ventricular Cardiomyocytes [48]

Digestion:

1. The perfusion buffer in the Eppendorf tube was replaced with digestion buffer (Table 2.1). For optimal results, 750 µl of the digestion buffer was used per tube (250 µl per heart).
2. The ventricles were then subjected to digestion in a thermomixer for 30–40 minutes at 32°C and 800 rpm. Older fish hearts needed a slightly longer time compared to the younger ones.

Wash:

1. Once the digestion was complete, the hearts were allowed to settle for a minute or two.
2. The digestion buffer was then replaced with 750 µl stopping buffer (Table 2.1), without disturbing the tissue at the bottom of the tube.
3. After 15 minutes in the stopping buffer, the supernatant buffer was replaced with fresh 750 µl stopping buffer or 750 µl plating medium, depending on the requirement. Cells in stopping buffer can survive for 4 hours but undergo minimal calcium-shock. Cells in plating medium were good for physiological measurements up to 10 hours but underwent calcium-shock, if not titrated with increasing concentrations of calcium.
4. The tissue was then gently triturated using a Pasteur pipette, to disperse the cells into solution.

Reagents:

- Collagenase Type II (Worthington)
- Collagenase Type IV (Worthington)
- Minimum Essential Medium (MEM; Gibco)
- GlutaMax (Gibco)
- 2,3-Butanedione Monoxime (BDM)
- Fetal Bovine Serum (FBS)
- Phosphate Buffer Saline (PBS)
- Glucose
- Taurine
- Bovine Serum Albumin (BSA)
- Calcium Chloride
- Insulin
- Penicillin-Streptomycin

Table 2.1 Solutions for Isolation of ZF Ventricular Cardiomyocytes

PERFUSION BUFFER (PB)	10 mM HEPES, 30 mM Taurine, 5.5 mM Glucose, 10 mM BDM
DIGESTION BUFFER (DB)	PB + 12.5 µM $CaCl_2$ + 5mg/ml Col II + 5mg/ml Col IV + 5 ng/ml Insulin
STOPPING BUFFER (SB)	PB + 10% FBS + 12.5 µM $CaCl_2$ + 10 mg/ml BSA + 5 ng/ml Insulin
PLATING MEDIUM (PM)	MEM + 2mM GlutaMax + 5mM BDM + 5% FBS + 100 U/mL Pen-Strep

2.2 Inside-Out Excised Patch-Clamping

Upon successful isolation of the ZF ventricular cardiomyocytes (VCMs), inside-out excised patch-clamping was performed to characterize K_{ATP} channel expression and activity, providing the first recordings of K_{ATP} currents in fish cardiomyocytes. The ZF VCMs, as discussed in chapter 3, are very slender and tiny in comparison to mammalian myocytes. This made them extremely sensitive to the continuous flow of buffers. Plating of the ZF VCMs on glass coverslips as per established protocols [48] proved to be futile. So, this turned out to be a flow-control challenge requiring the retooling of an old rig that uses a piezoresistive float-transducer to achieve sensitive flow control [49, 50]. This exercise proved very fruitful for the future experiments. A hydrophobic plastic-coated brass-shim 'float' is connected to the piezoresistive element via a thin metal tube and cyanoacrylic adhesive (Figure 2.3 a). The float assembly recognizes the fluid levels in the bath (Figure 2.3 b) through surface tension and relays it via a control circuit to the outflow pump (Figure 2.3 c), creating a feedback control loop. The bath consists of four channels, through which solutions supplied by inflow lines flow into a common end-pool and are pumped out through a single outflow. Cells are placed in the first channel (which is the widest; the numbering for channels is 1–4 from left–right), and patches are excised from these cells. A singular feature of this bath is that the columns separating the channels are provided with 'gates' filled with mineral oil, hence the chamber is referred to as an 'oil-gate chamber' within the 'oil-gate rig'. By moving the electrode tip from one channel to another through these oil-gates, the excised patch of the cell membrane can be exposed to different solutions flowing through them. Further, passing through oil provides an almost instantaneous change of solutions, which can be useful for studying the kinetics of the ion channels. The outflow pump motor is connected between the ground and 'motor' connections in the circuit, via a three-position switch from off to maximum to feedback control. In feedback mode, the float position determines the change in resistance of the piezoresistors (labelled with asterisk) which balance the circuit through a Wheatstone bridge.

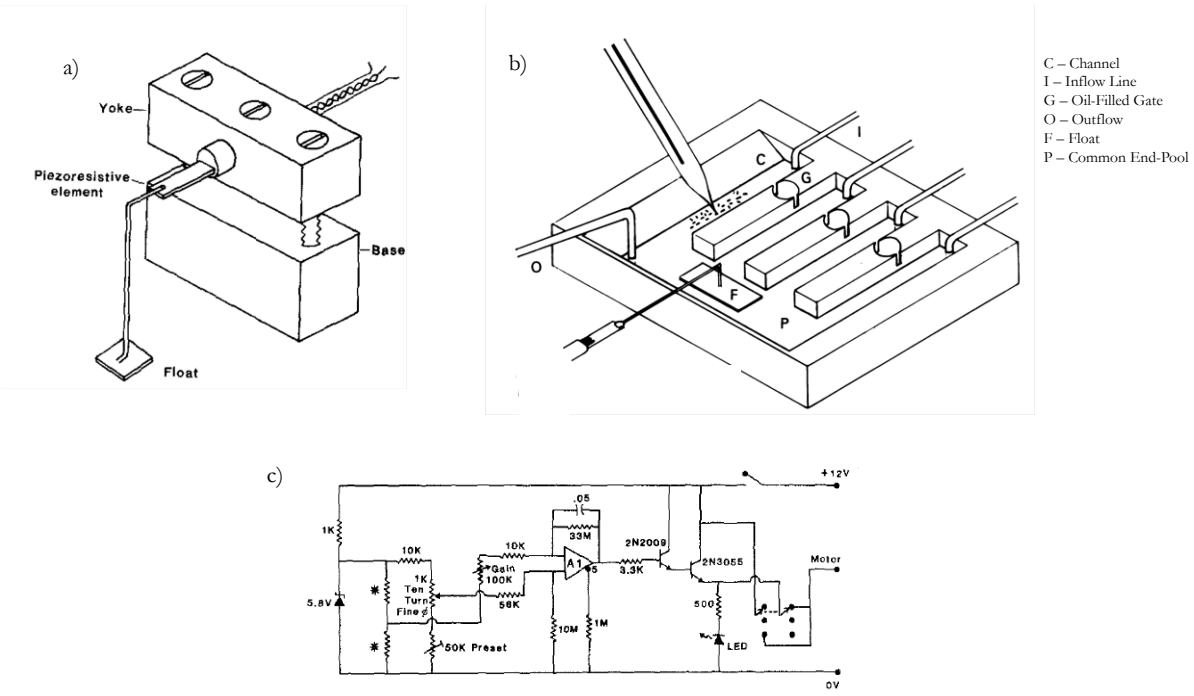

Figure 2.3 The Oil-Gate Rig
a) An oblique detailing of the float assembly [49] b) A schematic diagram of the oil-gate chamber [50]
c) Circuit diagram of the oil-gate rig's electrical control activity [49]

Micropipettes for patch-clamping were pulled from soda lime glass microhematocrit tubes (Kimble-Chase 2502) using a P-97 puller (Sutter Instruments) and had a resistance of 1–2 MΩ when filled with pipette solution. The pipette and channel 1 (also called Well 1) solutions typically contained K_{INT} (Table 2.2). Membrane currents were recorded at a constant holding potential of 50 mV, using an Axopatch 200B amplifier and Axon pCLAMP software from Molecular Devices. Experiments were performed at the room temperature (20–22 °C). Free Mg^{2+} concentrations for MgATP and MgADP dose-response recordings were calculated using CaBuf (Katholieke Universiteit Leuven). Channel currents in solutions of varying nucleotide concentrations were normalized to the basal current in the absence of nucleotides, and the dose-response data were fit with a four-parameter Hill fit according to equation 2.1, using the Data Solver Function in Microsoft Excel,

$$Normalized\ current = I_{min} + (I_{max} - I_{min})/(1 + ([X]/IC50)H) \qquad (2.1)$$

where the current in K_{INT} = I_{max} = 1; I_{min} is the normalized minimum current observed in Wells 2 or 4 (ATP/MgATP/glibenclamide); *[X]* refers to the concentration of the ATP/MgATP in the Well under consideration; IC50 is the concentration of half-maximal inhibition; and H denotes Hill coefficient.

Buffers for Patch-Clamping:

The KINT buffers, ATP buffers, Mg-nucleotide buffers and glibenclamide (GLB) buffers for ATP, MgATP and GLB dose-response recordings (DRRs) were prepared as per the following tables –

Table 2.2 K_{INT} Buffer (1 Liter)

SOLUTE	CONC.	SOLUTE ADDED	STOCK PREPARATION
KCl	140 mM	10.437 gms	MW: 74.5513 gm/mol
K.HEPES	10 mM	10 mL of 1 M Stock	23.83 gms of K.HEPES in 100 mL H_2O
K.EGTA	1 mM	2 mL of 0.5 M Stock	38.035 gms of K.EGTA in 200 mL H_2O
None of the stock solutions should contain Na, which blocks the K_{ATP} channels. Adjust the pH to 7.4 using only KOH, preferably pellets and makeup to 1 L.			

Table 2.3 Buffers for ATP DRR

WELL	BUFFER CONTENT	BUFFER PREPARATION
1	K_{INT}	50 mL of K_{INT} Solution
2	K_{INT} + 5 mM ATP	2.5 mL ATP Stock + 47.5 mL K_{INT} + Phenol Red
3	K_{INT} + 10 µM ATP	0.1 mL of Well 2 Buffer + 49.9 mL K_{INT}
4	K_{INT} + 100 µM ATP	1 mL of Well 2 Buffer + 49 mL K_{INT} + Phenol Red
ATP Stock: Freshly prepare 5 mL of 100 mM ATP stock by adding 0.291 gms of K.ATP in 4 mL K_{INT}, adjust the pH by using Phenol Red and KOH, makeup to 5 mL.		

Table 2.4 Buffers for MgATP DRR

WELL	BUFFER CONTENT	BUFFER PREPARATION
1	K_{INT}	50 mL of K_{INT} Solution
2	K_{INT} + 5 mM ATP + 4.65 mM $MgCl_2$	2.5 mL of ATP Stock + 2.325 mL $MgCl_2$ Stock + 45.175 mL K_{INT} + Phenol Red
3	K_{INT} + 10 µM ATP + 0.55 mM $MgCl_2$	0.1 mL of Well 2 Buffer + 0.270 mL $MgCl_2$ Stock + 49.629 mL K_{INT}
4	K_{INT} + 100 µM ATP + 0.62 mM $MgCl_2$	1 mL of Well 2 Buffer + 0.2635 mL $MgCl_2$ Stock + 48.7365 mL K_{INT} + Phenol Red
$MgCl_2$ Stock: Prepare 200 mL of 100 mM $MgCl_2$ stock by adding 4.066 gms of $MgCl_2.6H_2O$ in H_2O.		

Table 2.5 Buffers for GLB DRR

WELL	BUFFER CONTENT	BUFFER PREPARATION
1	K_{INT}	50 mL K_{INT} Solution
2	K_{INT} + 5 mM ATP + 4.65 mM $MgCl_2$	2.5 mL ATP Stock + 2.325 mL $MgCl_2$ Stock + 45.175 mL K_{INT} + Phenol Red
3	K_{INT} + 100 µM ATP + 0.96 mM $MgCl_2$ + 500 µM ADP	50 µL ATP Stock + 250 µL ADP Stock + 480 µL $MgCl_2$ Stock + 49.220 mL K_{INT}
4	K_{INT} + 100 µM ATP + 0.96 mM $MgCl_2$ + 500 µM ADP + 1 µM GLB	50 µL ATP Stock + 250 µL ADP Stock + 480 µL $MgCl_2$ Stock + 50 µL GLB Stock + 49.170 mL K_{INT}
GLB Stock: Prepare 10 mL of 1 mM GLB stock by dissolving 0.00494 gms of GLB in DMSO. ADP Stock: Prepare 5 mL of 100 mM ADP stock by adding 0.251 gms of K.ADP in 4 mL K_{INT}, adjust the pH by using Phenol Red and KOH, make up to 5 mL. Freeze & store in aliquots.		

2.3 Phenotypic Drug-Response Studies

In collaboration with Helen Roessler from UMC Utrecht, phenotypic drug-response studies using glibenclamide (GLB) were conducted in adult ZF and larvae to determine the sulfonylurea sensitivity of heart size in SUR2 mutated CS models of ZF. 10 adult fish each of wild type, G989E heterozygous and G989E homozygous were subjected to treatment with 50 μM GLB for two weeks. The 50 μM concentration of GLB was the maximum soluble drug in fish-water using 1% DMSO (Dimethyl sulfoxide). The drug was added to 1L of fish-water, which was exchanged once every day. In addition to the drug, 10 fish of each type were also subjected to 1% DMSO treatment as vehicle control and 10 others were each similarly used as controls in normal fish-water (E3). After two weeks of treatment, the hearts of the fish were excised and imaged using Hamamatsu C9300-221 high-speed CCD camera (Hamamatsu Photonics) at 150 frames per second (fps) mounted on a Leica DM IRBE inverted microscope (Leica Microsystems) using Hokawo 2.1 imaging software (Hamamatsu Photonics). Subsequent image analysis was carried out using NIH's image processing program, ImageJ.

The imaging was done for approximately 10 seconds at room temperature (28 ^{o}C).

Chapter 3

Results and Discussion

3.1 Phenotypic Characterization of CS Fish

In collaboration A phenotypic characterization of the cardiovascular phenotypes of CS in ZF, such as enlarged ventricles, enhanced cardiac output and contractile function, cerebral vasodilation has been performed in one of the earlier studies by Helen Roessler from UMC Utrecht, confirming an efficient introduction of the GOF mutations (Figure 3.1) [40].

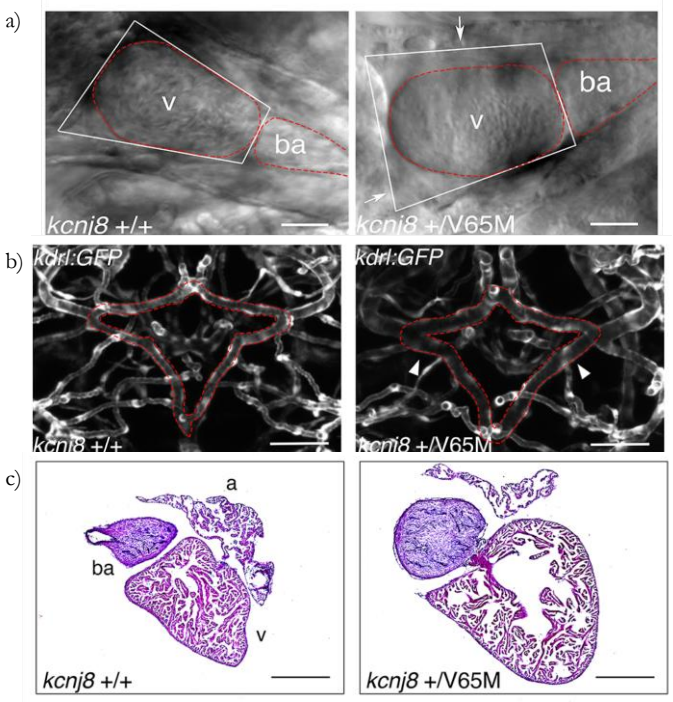

Figure 3.1 Phenotypic Characterization of CS in ZF [40]
a) Confocal imaging used to assess the cardiac function 5dpf b) Cerebral vasodilation in WT and mutant ZF, 5dpf c) H&E staining showing the enlarged ventricular size in ZF, 5dpf

It was reported in those studies that the C1043Y mutation had less severe cardiovascular phenotypes compared to the G989E mutation. One conceivable explanation can be found in the positioning of these mutations. G989E is situated closer to the sulfonylurea (GLB) drug-binding site, whose Cryo-EM structure was recently resolved [51] and on the side chain directly connecting the NBD1 to the TMD of the SUR subunit, whereas C1043Y is situated at the extracellular face of TMD (Figure 3.2).

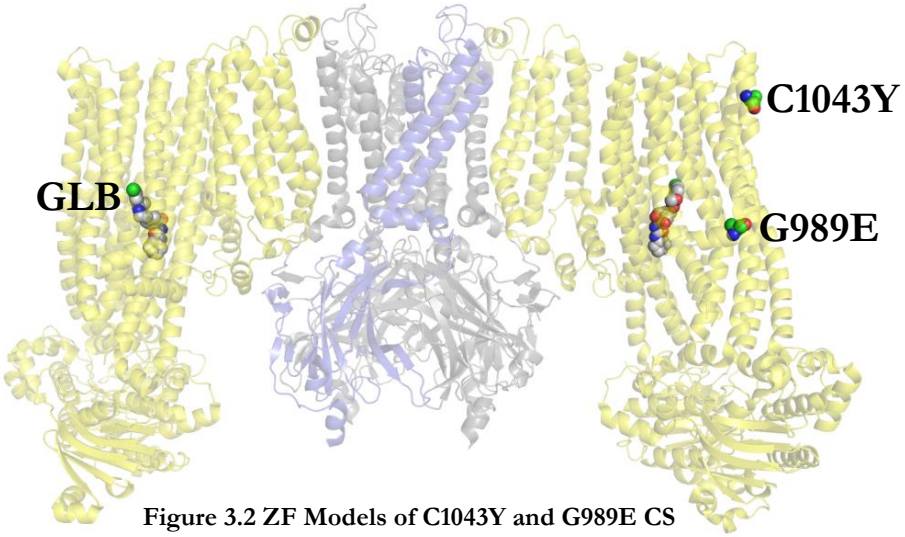

Figure 3.2 ZF Models of C1043Y and G989E CS
Structural representation of the ventricular cardiomyocyte K_{ATP} channel with the equivalent position of C1043Y and G989E mutations in SUR2 domain, relative to the GLB binding site.

3.2 Zebrafish Ventricular Cardiomyocytes

The protocol developed in the chapter 2 for isolating ZF ventricular cardiomyocytes (VCMs) uses 3 fish, takes 1 hour for the isolation and yields 80% live cells (Figure 3.3 b). ZF ventricular cardiomyocytes are very tiny in comparison to their murine counterparts and are difficult to patch-clamp with microelectrode tips lower than 1 MΩ resistance (when filled with K_{INT} solution) (Figure 3.3 a, c). Non-plated cells almost always are pulled with the electrode, making it necessary to go into oil or air for the excision. Also, resealing at the tip upon excision (formation of vesicles) was very frequent for ZF VCMs, at times requiring long periods of exposure to air outside the buffer for the inside-out configuration to be achieved.

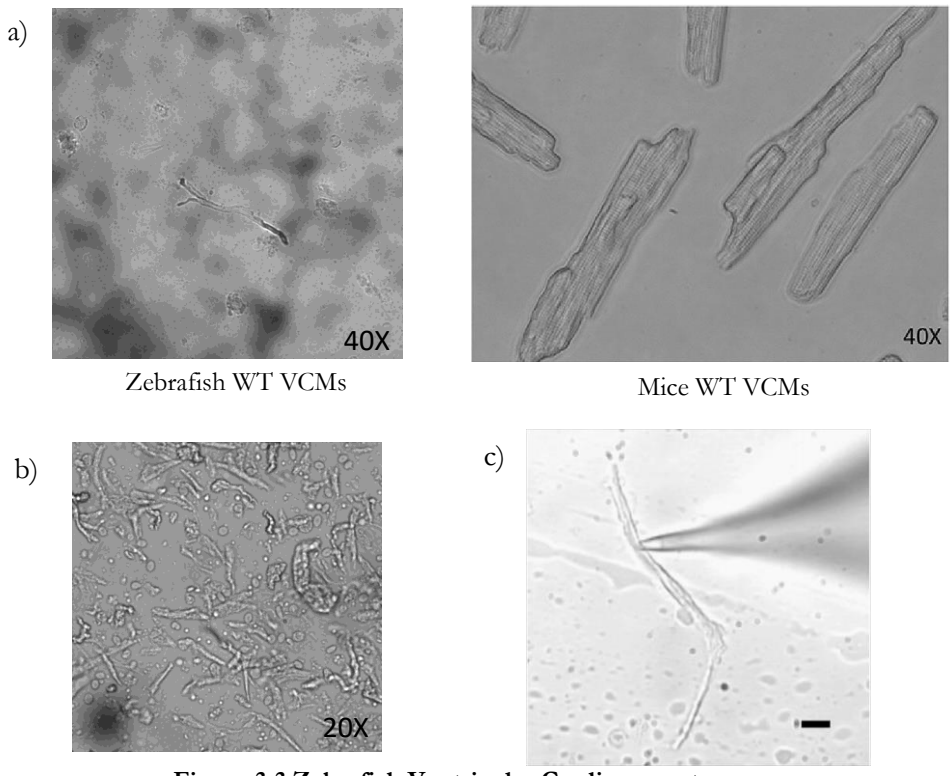

Figure 3.3 Zebrafish Ventricular Cardiomyocytes
a) A wildtype ZF VCM compared with mice VCMs at 40x b) The density and quality of ZF VCMs obtained using the developed isolation protocol c) Size-comparison of a ZF VCM with a microelectrode tip attached to it, scale bar is 5 μm [46]

3.3 ATP-Sensitivity of CS ZF VCM K_{ATP}

The ATP dose-response recordings from ZF VCMs, show a typical K_{ATP} channel activity (Figure 3.4) with ~4 pA single channel current at +50 mV in the buffer conditions used, corresponding to 80 pS single channel conductance, and a rapid inhibition of the channel current by intracellular ATP (5 mM). In low concentration of ATP (10 μM), channel activity was ~ 80% of maximum in the WT, 85% in the heterozygous and ~90% in the homozygous C1043Y and G989E channels, suggesting a decreased sensitivity to inhibitory ATP, which was also evident in moderate concentrations of ATP (100 μM).

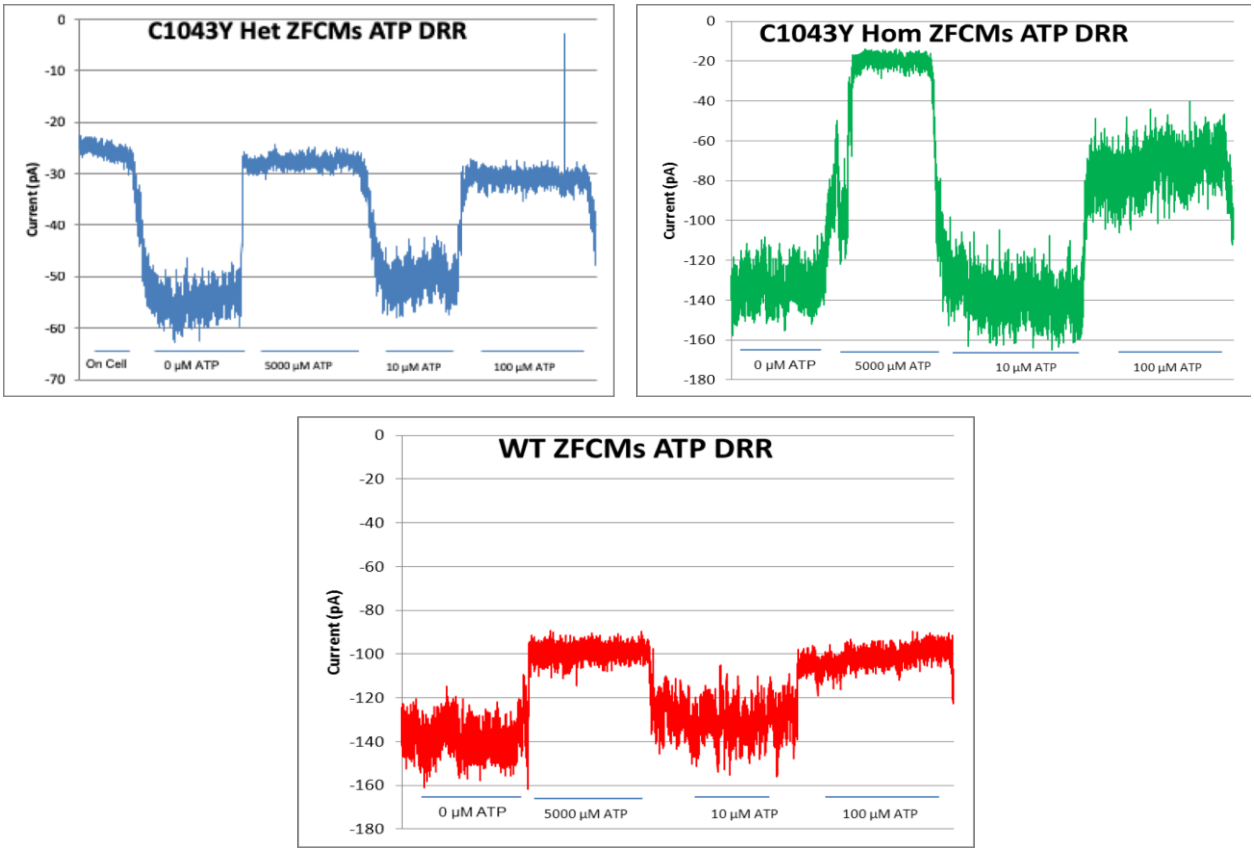

Figure 3.4 K_{ATP} Channels in WT and C1043Y
Representative inside-out patch-clamp recordings of K_{ATP} channel activity from ZF VCMs of WT, C1043Y heterozygous and homozygous mutants.

This decreased sensitivity is characterized by the increase in IC_{50} values for the C1043Y and G989E mutants (Figure 3.5, 3.6). The amount of ATP required to cause 50% inhibition of the channels (IC_{50}) for the C1043Y and G989E homozygous mutants was ~60 μM and ~40 μM respectively. The IC_{50} values for the C1043Y and G989E heterozygous mutants were ~17 μM and ~23 μM respectively, whereas the WT IC_{50} value was ~16 μM.

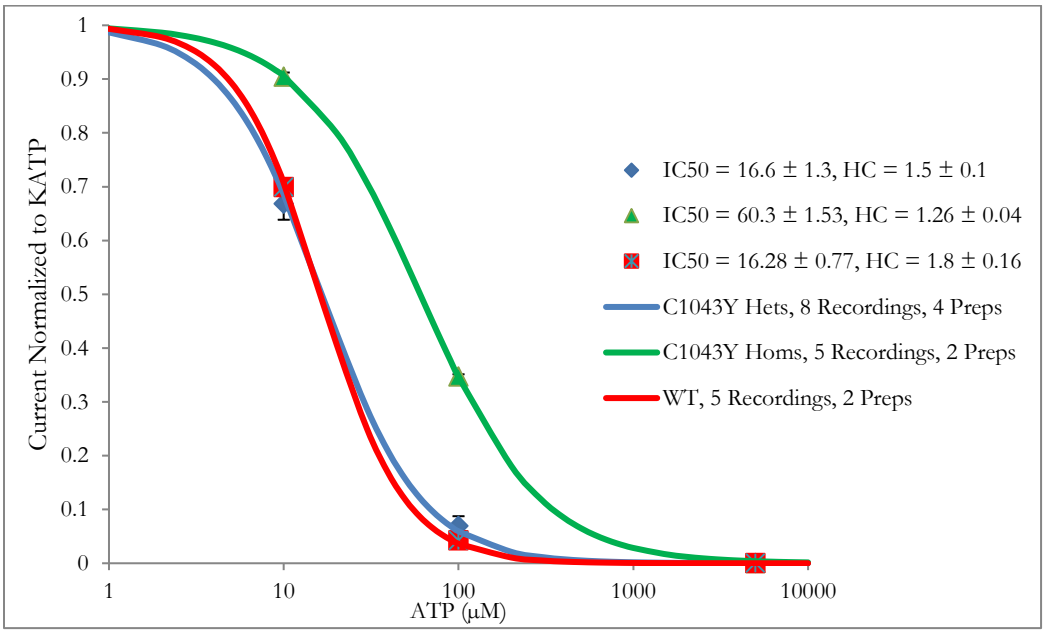

Figure 3.5 C1043Y ATP DRC
Summary ATP dose-response curves for C1043Y homozygous and heterozygous mutants

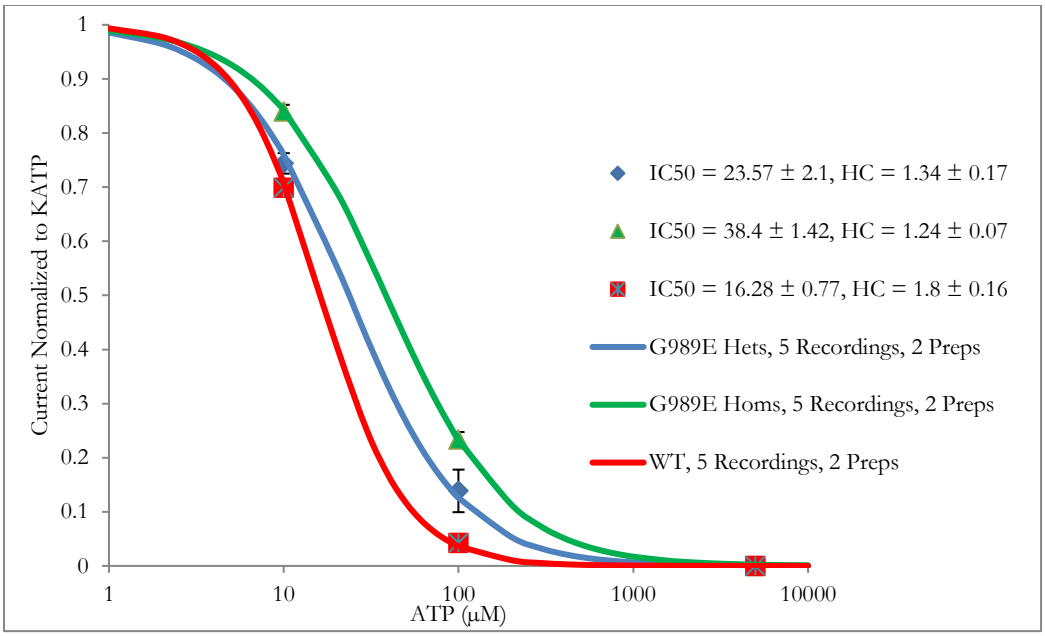

Figure 3.6 G989E ATP DRC

Summary ATP dose-response curves for G989E homozygous and heterozygous mutants

The introduced mutations could result in reduced ATP-sensitivity by several potential mechanisms: stabilization of the channel in the open state, thereby increasing the open probability (P_o) may be the most reasonable, rather than directly affecting the inhibitory ATP-binding, since the inhibitory ATP-binding site is on the pore-forming (Kir6.x) subunit. Activating nucleotides interact with SUR, but in a Mg-dependent manner, and the above experiments were carried out in the absence of Mg^{2+}.

3.4 ATP-Sensitivity in the Presence of Mg^{2+}

To further investigate the effects of the induced mutations on SUR2-dependent nucleotide interactions, MgATP dose-responses were assessed, as described in chapter 2. A further rightward shift in ATP sensitivity was seen in the presence of Mg, for both the G989E and C1043Y mutant channels, compared to Mg-free conditions (Figure 3.7, 3.8 and 3.9).

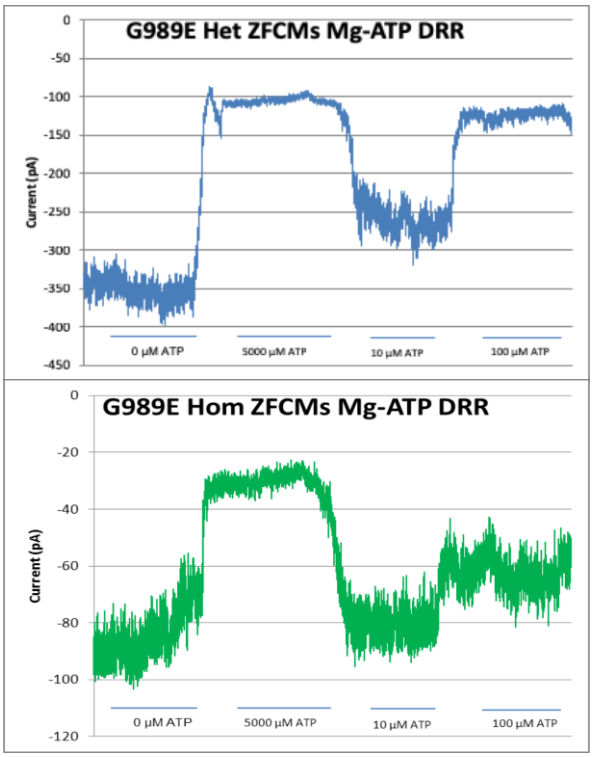

Figure 3.7 MgATP DRR in G989E
Representative inside-out patch-clamp recordings of K_{ATP} channel activity from ZF VCMs of G989E heterozygous and homozygous mutants in the presence of MgATP.

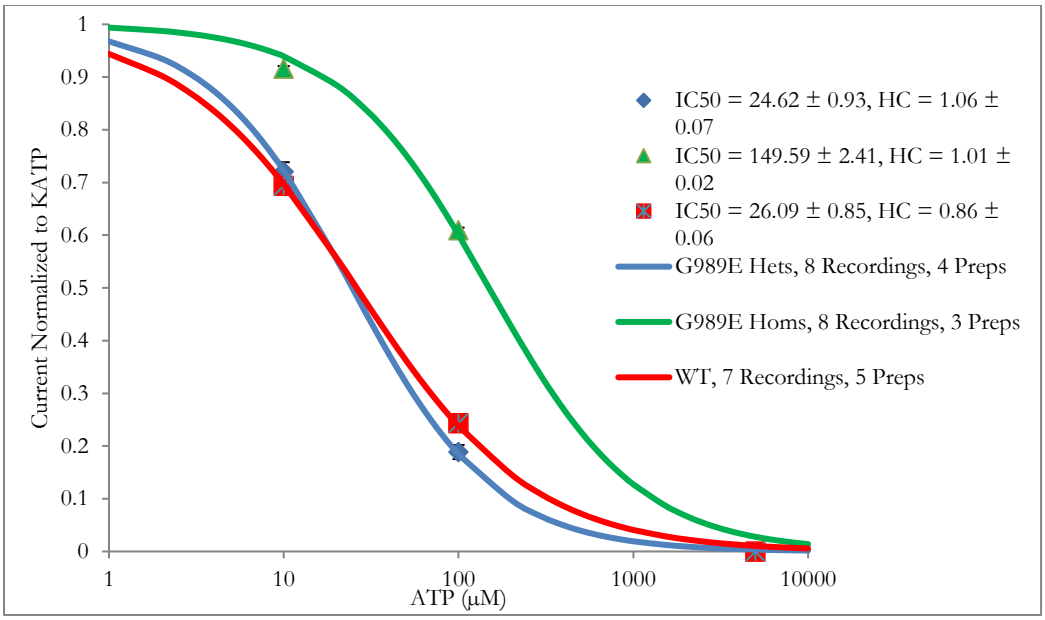

Figure 3.8 G989E MgATP DRC

Summary MgATP dose-response curves for G989E homozygous and heterozygous mutants

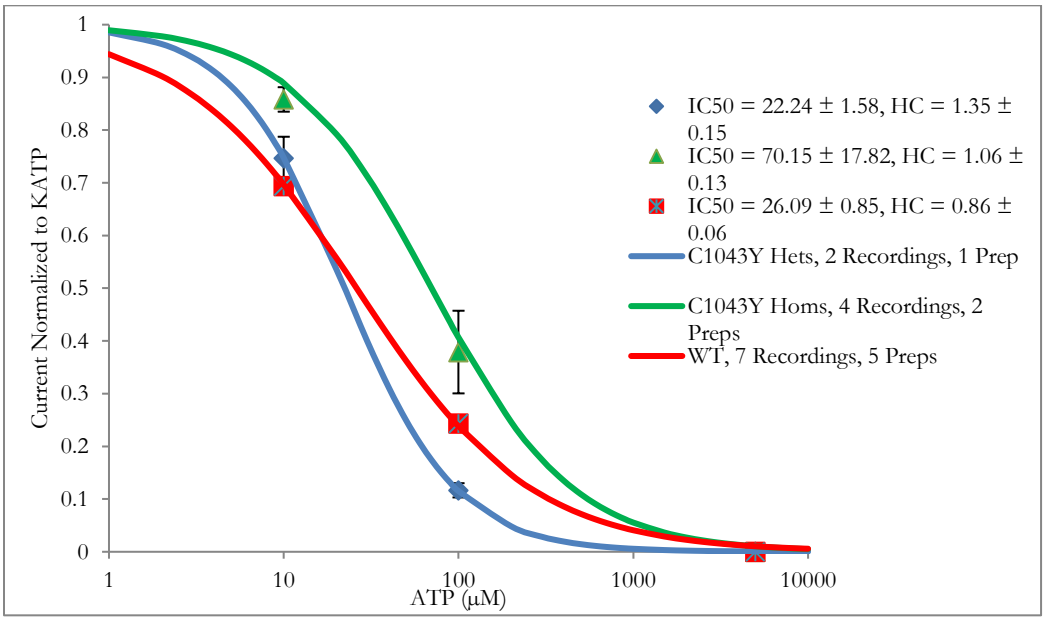

Figure 3.9 C1043Y MgATP DRC

Summary MgATP dose-response curves for C1043Y homozygous and heterozygous mutants

The IC_{50} values for G989E homozygous increased by about 110 μM in MgATP compared to ATP, whereas the shift was only about 10 μM in C1043Y homozygous and WT. Due to the low number of recordings obtained, shifts in the heterozygous were less clear. G989E proved to be the more sever mutation at the organ level, with larger hearts than C1043Y [40], and the more marked right-shift of IC_{50} curves for G989E suggests that Mg-nucleotide interaction or consequence may be additionally affected in this case, perhaps due to the close proximity of this residue to the nucleotide binding domain (Figure 3.2). A more marked gain-of-function (GOF) for this mutation is consistent with data from previous studies using transfected cells [9, 52]. Another interesting anecdotal observation was that the quality of isolated cells, and channel density seem to be proportional to the K_{ATP} channel activity. Homozygous mutants consistently gave better quality cells and more channels per excision, compared to the WT controls that were isolated and patched simultaneously. This could be due to the ischemic protection offered by K_{ATP} channels in the cardiomyocytes.

3.5 Glibenclamide Sensitivity

Second-generation sulfonylureas such as glibenclamide (GLB) bind to the SUR subunits of K_{ATP} channels and cause an inhibitory action [53]. This presents a potential pharmacotherapeutic option for CS. However, multiple reports suggest that, in other tissues, such GOF mutations, by increasing the open state stability, also reduce the sulfonylurea sensitivity [54-57]. To assess the effect of SUR2 CS mutations on inhibitor sensitivity, GLB dose-response studies were performed as described in chapter 2. A decrease in GLB potency was seen in both C1043Y and G989E mutations (Figure 3.10). The insensitivity seemed to be inversely proportional to the severity of the mutation, with G989E homozygous reporting around 20% inhibition compared to 30% and 80% in C1043Y homozygous and WT, with the heterozygous of G989E and C1043Y lying in between 45% and 55%.

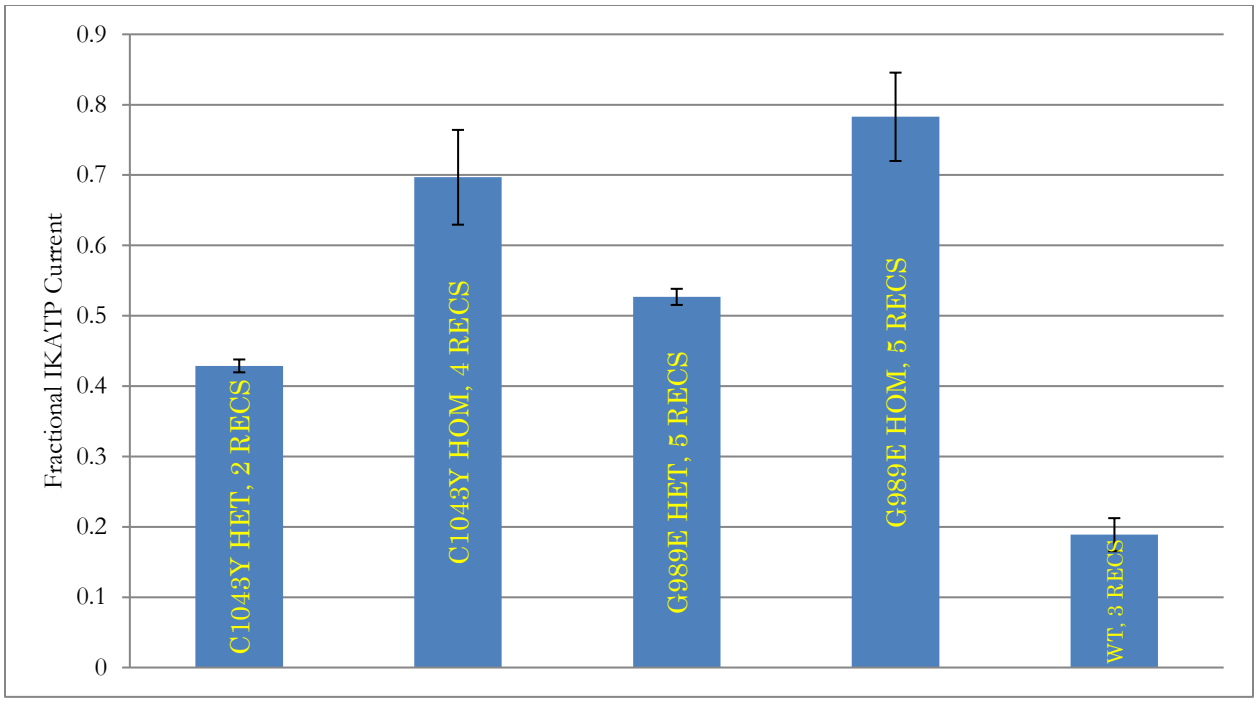

Figure 3.10 GLB Response Study

The fractional K_{ATP} current remaining in the presence of 10 μM Glibenclamide (GLB) in the inside-out patch clamp recordings from zebrafish VCMs.

The GLB sensitivity was evaluated in a 'homozygous' context. However, since all CS patients identified so far are heterozygous, the treatability of the disease using GLB still needs to be evaluated and a phenotypic drug-response study was conducted using the methods described in chapter 2. G989E was chosen as the model for the study, due to its phenotypic severity. After two weeks of treatment, cardiomegaly – a predominant cardiovascular phenotype for CS, was analyzed. The heart size inclined towards reduction in both the homozygous and heterozygous case (Figure 3.11).

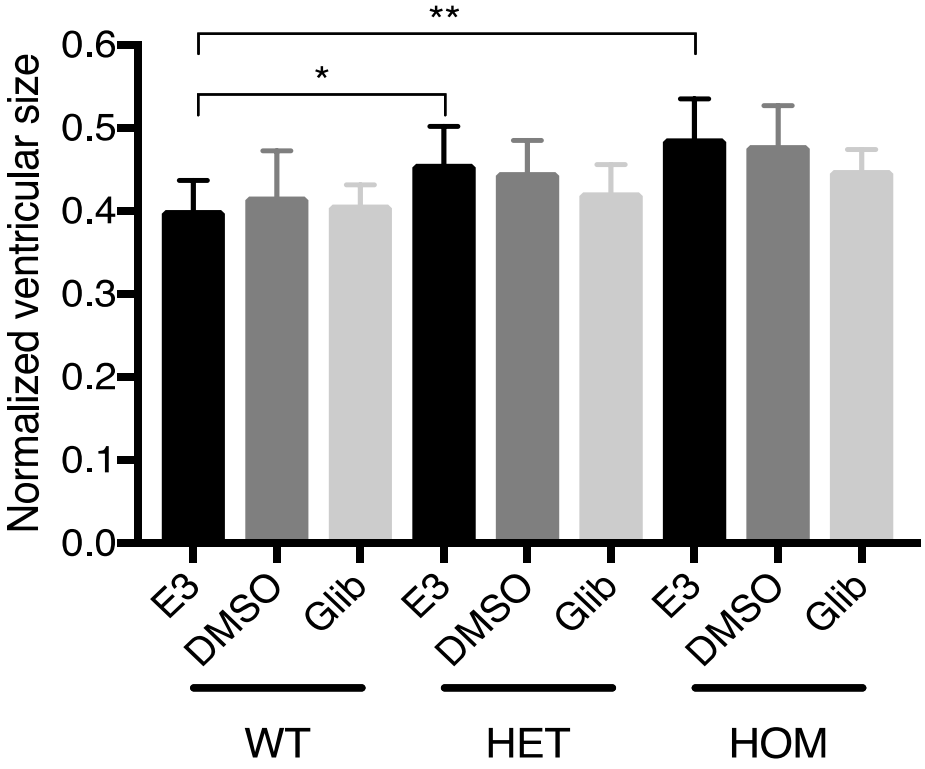

Figure 3.11 Phenotypic GLB Dose-Response Study in G989E

Chapter 4

Conclusion

Taken together, these results validate the gain-of-function at a molecular and cellular level in the ventricular cardiomyocytes of zebrafish models of Cantú syndrome. Given that these are also the first recordings of K_{ATP} currents from ZF cardiomyocytes, they also serve to provide a basis for the characterization of K_{ATP} channel composition in ZF. Using *ABCC9* and *ABCC8* knock-out fish, the channel composition in the atrial and ventricular cardiomyocytes can be determined. Also, using *KCNJ8* and *KCNJ11* knock-out fish, the functional significance of Kir6.3, which is unique to the teleost can be determined. In this regard, the retooled oil-gate rig will continue to serve an important function in determining further channel activities. The developed isolation protocol may also be adapted for successful isolation of atrial cardiomyocytes, and for vascular smooth muscle (VSM) cells, which would give further insights into the cardiovascular mechanisms involved in CS. The successful isolation and characterization of the channels in VSM cells will prove valuable in studying *KCNJ8* models of CS. This would help in further validation of the fish models, which with all the advantages listed in chapter 1, promise an exciting future for research into Cantú syndrome and other cardiovascular diseases.

References

[1] Ericsson, A.C., Crim, M.J. and Franklin, C.L., 2013. A brief history of animal modeling. *Missouri medicine*, *110*(3), p.201.

[2] Grange, D.K., Nichols, C.G. and Singh, G.K., 2014. Cantú syndrome and related disorders.

[3] Nichols, C.G., Singh, G.K. and Grange, D.K., 2013. KATP channels and cardiovascular disease: suddenly a syndrome. *Circulation research*, *112*(7), pp.1059-1072.

[4] Van Bon, B.W., Gilissen, C., Grange, D.K., Hennekam, R.C., Kayserili, H., Engels, H., Reutter, H., Ostergaard, J.R., Morava, E., Tsiakas, K. and Isidor, B., 2012. Cantu syndrome is caused by mutations in ABCC9. *The American Journal of Human Genetics*, *90*(6), pp.1094-1101.

[5] Harakalova, M., van Harssel, J.J., Terhal, P.A., van Lieshout, S., Duran, K., Renkens, I., Amor, D.J., Wilson, L.C., Kirk, E.P., Turner, C.L. and Shears, D., 2012. Dominant missense mutations in ABCC9 cause Cantu syndrome. *Nature genetics*, *44*(7), p.793.

[6] Brownstein, C.A., Towne, M.C., Luquette, L.J., Harris, D.J., Marinakis, N.S., Meinecke, P., Kutsche, K., Campeau, P.M., Timothy, W.Y., Margulies, D.M. and Agrawal, P.B., 2013. Mutation of KCNJ8 in a patient with Cantú syndrome with unique vascular abnormalities–Support for the role of K (ATP) channels in this condition. *European journal of medical genetics*, *56*(12), pp.678-682.

[7] Cooper, P.E., Reutter, H., Woelfle, J., Engels, H., Grange, D.K., van Haaften, G., van Bon, B.W., Hoischen, A. and Nichols, C.G., 2014. Cantú Syndrome Resulting from Activating Mutation in the KCNJ 8 Gene. *Human mutation*, *35*(7), pp.809-813.

[8] Cooper, P.E., McClenaghan, C., Chen, X., Stary-Weinzinger, A. and Nichols, C.G., 2017. Conserved functional consequences of disease-associated mutations in the slide-helix of Kir6. 1 and Kir6. 2 subunits of the ATP-sensitive potassium channel. *Journal of Biological Chemistry*, pp.jbc-M117.

[9] McClenaghan, C., Hanson, A., Sala-Rabanal, M., Roessler, H.I., Josifova, D., Grange, D.K., van Haaften, G. and Nichols, C.G., 2018. Cantu syndrome–associated SUR2 (ABCC9) mutations in distinct structural domains result in KATP channel gain-of-function by differential mechanisms. *Journal of Biological Chemistry*, *293*(6), pp.2041-2052.

[10] Huang, Y., McClenaghan, C., Harter, T.M., Hinman, K., Halabi, C.M., Matkovich, S.J., Zhang, H., Brown, G.S., Mecham, R.P., England, S.K. and Kovacs, A., 2018. Cardiovascular consequences of KATP overactivity in Cantu syndrome. *JCI insight*, *3*(15).

[11] Camacho, P., Fan, H., Liu, Z. and He, J.Q., 2016. Small mammalian animal models of heart disease. *American journal of cardiovascular disease*, *6*(3), p.70.

[12] Inagaki, N., Gonoi, T., Iv, J.P.C., Wang, C.Z., Aguilar-Bryan, L., Bryan, J. and Seino, S., 1996. A family of sulfonylurea receptors determines the pharmacological properties of ATP-sensitive K+ channels. Neuron, 16(5), pp.1011-1017.

[13] Isomoto, S., Kondo, C., Yamada, M., Matsumoto, S., Higashiguchi, O., Horio, Y., Matsuzawa, Y. and Kurachi, Y., 1996. A novel sulfonylurea receptor forms with BIR (Kir6. 2) a smooth muscle type ATP-sensitive K+ channel. Journal of Biological Chemistry, 271(40), pp.24321-24324.

[14] Chutkow, W.A., Simon, M.C., Le Beau, M.M. and Burant, C.F., 1996. Cloning, tissue expression, and chromosomal localization of SUR2, the putative drug-binding subunit of cardiac, skeletal muscle, and vascular KATP channels. Diabetes, 45(10), pp.1439-1445.

[15] Shyng, S.L. and Nichols, C.G., 1997. Octameric stoichiometry of the KATP channel complex. The Journal of general physiology, 110(6), pp.655-664.

[16] Clement IV, J.P., Kunjilwar, K., Gonzalez, G., Schwanstecher, M., Panten, U., Aguilar-Bryan, L. and Bryan, J., 1997. Association and stoichiometry of KATP channel subunits. Neuron, 18(5), pp.827-838.

[17] Martin, G.M., Yoshioka, C., Rex, E.A., Fay, J.F., Xie, Q., Whorton, M.R., Chen, J.Z. and Shyng, S.L., 2017. Cryo-EM structure of the ATP-sensitive potassium channel illuminates mechanisms of assembly and gating. Elife, 6, p.e24149.

[18] Li, N., Wu, J.X., Ding, D., Cheng, J., Gao, N. and Chen, L., 2017. Structure of a pancreatic ATP-sensitive potassium channel. Cell, 168(1-2), pp.101-110.

[19] Nichols, C.G., 2006. K ATP channels as molecular sensors of cellular metabolism. Nature, 440(7083), p.470.

[20] Tucker, S.J., Gribble, F.M., Zhao, C., Trapp, S. and Ashcroft, F.M., 1997. Truncation of Kir6. 2 produces ATP-sensitive K+ channels in the absence of the sulphonylurea receptor. Nature, 387(6629), pp.179-183.

[21] Nichols, C.G., Shyng, S.L., Nestorowicz, A., Glaser, B., Clement, J.T., Gonzalez, G., Aguilar-Bryan, L., Permutt, M.A. and Bryan, J., 1996. Adenosine diphosphate as an intracellular regulator of insulin secretion. Science, 272(5269), pp.1785-1787.

[22] Flagg, T.P., Kurata, H.T., Masia, R., Caputa, G., Magnuson, M.A., Lefer, D.J., Coetzee, W.A. and Nichols, C.G., 2008. Differential structure of atrial and ventricular KATP: atrial KATP channels require SUR1. Circulation research, 103(12), pp.1458-1465.

[23] Foster, M.N. and Coetzee, W.A., 2015. KATP channels in the cardiovascular system. Physiological reviews, 96(1), pp.177-252.

[24] Flagg, T.P., Enkvetchakul, D., Koster, J.C. and Nichols, C.G., 2010. Muscle KATP channels: recent insights to energy sensing and myoprotection. Physiological reviews, 90(3), pp.799-829.

[25] Li, A., Knutsen, R.H., Zhang, H., Osei-Owusu, P., Moreno-Dominguez, A., Harter, T.M., Uchida, K., Remedi, M.S., Dietrich, H.H., Bernal-Mizrachi, C. and Blumer, K.J., 2013. Hypotension due to Kir6. 1 gain-of-function in vascular smooth muscle. Journal of the American Heart Association, 2(4), p.e000365.

[26] Tinker, A., Aziz, Q. and Thomas, A., 2014. The role of ATP-sensitive potassium channels in cellular function and protection in the cardiovascular system. British journal of pharmacology, 171(1), pp.12-23.

[27] Cole, W.C., McPherson, C.D. and Sontag, D., 1991. ATP-regulated K+ channels protect the myocardium against ischemia/reperfusion damage. Circulation Research, 69(3), pp.571-581.

[28] Suzuki, M., Sasaki, N., Miki, T., Sakamoto, N., Ohmoto-Sekine, Y., Tamagawa, M., Seino, S., Marbán, E. and Nakaya, H., 2002. Role of sarcolemmal K ATP channels in cardioprotection against ischemia/reperfusion injury in mice. The Journal of clinical investigation, 109(4), pp.509-516.

[29] Nelson, M.T., Huang, Y., Brayden, J.E., Hescheler, J. and Standen, N.B., 1990. Arterial dilations in response to calcitonin gene-related peptide involve activation of K+ channels. Nature, 344(6268), p.770.

[30] Nakashima, M. and Vanhoutte, P.M., 1995. Isoproterenol causes hyperpolarization through opening of ATP-sensitive potassium channels in vascular smooth muscle of the canine saphenous vein. Journal of Pharmacology and Experimental Therapeutics, 272(1), pp.379-384.

[31] Bonev, A.D. and Nelson, M.T., 1993. Muscarinic inhibition of ATP-sensitive K+ channels by protein kinase C in urinary bladder smooth muscle. American Journal of Physiology-Cell Physiology, 265(6), pp.C1723-C1728.

[32] Ko, E.A., Han, J., Jung, I.D. and Park, W.S., 2008. Physiological roles of K+ channels in vascular smooth muscle cells. Journal of Smooth Muscle Research, 44(2), pp.65-81.

[33] Teramoto, N., 2006. Physiological roles of ATP-sensitive K+ channels in smooth muscle. The Journal of physiology, 572(3), pp.617-624.

[34] Howe, K., Clark, M.D., Torroja, C.F., Torrance, J., Berthelot, C., Muffato, M., Collins, J.E., Humphray, S., McLaren, K., Matthews, L. and McLaren, S., 2013. The zebrafish reference genome sequence and its relationship to the human genome. Nature, 496(7446), p.498.

[35] Hodgson, P., Ireland, J. and Grunow, B., 2018. Fish, the better model in human heart research? Zebrafish Heart aggregates as a 3D spontaneously cardiomyogenic in vitro model system. Progress in biophysics and molecular biology.

[36] van Opbergen, C.J., van der Voorn, S.M., Vos, M.A., de Boer, T.P. and van Veen, T.A., 2018. Cardiac Ca 2+ signalling in zebrafish: Translation of findings to man. Progress in biophysics and molecular biology.

[37] Vornanen, M. and Hassinen, M., 2016. Zebrafish heart as a model for human cardiac electrophysiology. Channels, 10(2), pp.101-110.

[38] Nemtsas, P., Wettwer, E., Christ, T., Weidinger, G. and Ravens, U., 2010. Adult zebrafish heart as a model for human heart? An electrophysiological study. Journal of molecular and cellular cardiology, 48(1), pp.161-171.

[39] Poss, K.D., 2007, February. Getting to the heart of regeneration in zebrafish. In Seminars in cell & developmental biology (Vol. 18, No. 1, pp. 36-45). Academic Press.

[40] Tessadori, F., Roessler, H.I., Savelberg, S.M., Chocron, S., Kamel, S.M., Duran, K.J., van Haelst, M.M., van Haaften, G. and Bakkers, J., 2018. Effective CRISPR/Cas9-based nucleotide editing in zebrafish to model human genetic cardiovascular disorders. Disease models & mechanisms, 11(10), p.dmm035469.

[41] Zhang, C., Miki, T., Shibasaki, T., Yokokura, M., Saraya, A. and Seino, S., 2006. Identification and characterization of a novel member of the ATP-sensitive K+ channel subunit family, Kir6. 3, in zebrafish. Physiological genomics, 24(3), pp.290-297.

[42] Nam, Y.H., Hong, B.N., Rodriguez, I., Ji, M.G., Kim, K., Kim, U.J. and Kang, T.H., 2015. Synergistic potentials of coffee on injured pancreatic islets and insulin action via KATP

channel blocking in zebrafish. Journal of agricultural and food chemistry, 63(23), pp.5612-5621.

[43] Capiotti, K.M., Junior, R.A., Kist, L.W., Bogo, M.R., Bonan, C.D. and Da Silva, R.S., 2014. Persistent impaired glucose metabolism in a zebrafish hyperglycemia model. Comparative Biochemistry and Physiology Part B: Biochemistry and Molecular Biology, 171, pp.58-65.

[44] Emfinger, C.H., Welscher, A., Yan, Z., Wang, Y., Conway, H., Moss, J.B., Moss, L.G., Remedi, M.S. and Nichols, C.G., 2017. Expression and function of ATP-dependent potassium channels in zebrafish islet β-cells. Royal Society open science, 4(2), p.160808.

[45] Hassinen, M., Haverinen, J., Hardy, M.E., Shiels, H.A. and Vornanen, M., 2015. Inward rectifier potassium current (I K1) and Kir2 composition of the zebrafish (Danio rerio) heart. Pflügers Archiv-European Journal of Physiology, 467(12), pp.2437-2446.

[46] Brette, F., Luxan, G., Cros, C., Dixey, H., Wilson, C. and Shiels, H.A., 2008. Characterization of isolated ventricular myocytes from adult zebrafish (Danio rerio). Biochemical and biophysical research communications, 374(1), pp.143-146.

[47] Louch, W.E., Sheehan, K.A. and Wolska, B.M., 2011. Methods in cardiomyocyte isolation, culture, and gene transfer. Journal of molecular and cellular cardiology, 51(3), pp.288-298.

[48] Sander, V., Suñe, G., Jopling, C., Morera, C. and Belmonte, J.C.I., 2013. Isolation and in vitro culture of primary cardiomyocytes from adult zebrafish hearts. Nature protocols, 8(4), p.800.

[49] Cannell, M.B. and Lederer, W.J., 1986. A novel experimental chamber for single-cell voltage-clamp and patch-clamp applications with low electrical noise and excellent temperature and flow control. Pflügers Archiv, 406(5), pp.536-539.

[50] Lederer, W.J. and Nichols, C.G., 1989. Nucleotide modulation of the activity of rat heart ATP-sensitive K+ channels in isolated membrane patches. The Journal of Physiology, 419(1), pp.193-211.

[51] Martin, G.M., Kandasamy, B., DiMaio, F., Yoshioka, C. and Shyng, S.L., 2017. Anti-diabetic drug binding site in a mammalian KATP channel revealed by Cryo-EM. Elife, 6, p.e31054.

[52] Cooper, P.E., Sala-Rabanal, M., Lee, S.J. and Nichols, C.G., 2015. Differential mechanisms of Cantú syndrome–associated gain of function mutations in the ABCC9 (SUR2) subunit of the KATP channel. The Journal of general physiology, 146(6), pp.527-540.

[53] Gribble, F.M., Tucker, S.J., Seino, S. and Ashcroft, F.M., 1998. Tissue specificity of sulfonylureas: studies on cloned cardiac and beta-cell K (ATP) channels. Diabetes, 47(9), pp.1412-1418.

[54] Koster, J.C., Remedi, M.S., Dao, C. and Nichols, C.G., 2005. ATP and sulfonylurea sensitivity of mutant ATP-sensitive K+ channels in neonatal diabetes: implications for pharmacogenomic therapy. Diabetes, 54(9), pp.2645-2654.

[55] Proks, P., 2013. Neonatal diabetes caused by activating mutations in the sulphonylurea receptor. Diabetes & metabolism journal, 37(3), pp.157-164.

[56] Hambrock, A., Löffler-Walz, C. and Quast, U., 2002. Glibenclamide binding to sulphonylurea receptor subtypes: dependence on adenine nucleotides. British journal of pharmacology, 136(7), pp.995-1004.

[57] Proks, P., de Wet, H. and Ashcroft, F.M., 2014. Sulfonylureas suppress the stimulatory action of Mg-nucleotides on Kir6. 2/SUR1 but not Kir6. 2/SUR2A KATP channels: a mechanistic study. The Journal of general physiology, 144(5), pp.469-486.